

Interannual variability of extratropical transient wave activity and its influence on rainfall over Uruguay

Marcelo Barreiro* 

Departamento de Ciencias de la Atmósfera, Facultad de Ciencias, Universidad de la Republica, Montevideo, Uruguay

ABSTRACT: We explore the interannual variability of summertime extratropical transient activity and assess its influence on rainfall over southeastern South America focusing on Uruguay. Transient wave activity is characterized calculating the group velocity using daily mean meridional velocity at 300 hPa.

It is found that transient activity shows strong interannual variability consisting in patterns that represent a strengthening of wave activity in the subtropical Pacific, and meridional shifts in the position of the Pacific and Atlantic storm tracks. Part of the variability is associated with El Niño, which strongly influences northern Uruguay. Rainfall in southern Uruguay is correlated with latitudinal shifts in transient wave activity such that a strengthening in transient energy between 35° and 45°S extending from the southeastern Pacific into the South American continent favours positive anomalies.

For El Niño to induce increased rainfall over southern Uruguay it has to force two stationary waves: one that emanates from central Pacific describing an arch of low curvature into high latitudes and then towards the south Atlantic and another shorter wave that emanates from the eastern Pacific turning north-eastward at the latitude of the subtropical jet. When the latter is strong, surface northerlies reach southern Uruguay destabilizing the atmosphere due to enhanced transport of moisture and warm air. Coincident changes in transient wave activity south of 35°S increases the associated frontal activity and thus can induce positive rainfall anomalies by tapping the increased available moisture. In this case, the sea surface temperature (SST) anomalies are maximum in the central equatorial Pacific. On the other hand, a warmer eastern Pacific generates a stationary wave that shifts the subtropical jet northward increasing rainfall over south Brazil and decreasing it to the south of Uruguay. Thus, the summertime influence of El Niño over southern Uruguay is strongly dependent on the pattern of equatorial Pacific SST anomalies.

KEY WORDS atmospheric transient activity; rainfall; Uruguay; El Niño

1. Introduction

Subtropical South America to the east of the Andes is a transition region between the central part of the continent where rainfall is produced mainly by deep moist convection and the southern part where frontal systems play a major role in organizing deep convection producing most of the precipitation (Lenters and Cook, 1995; Garreaud and Wallace, 1998). Within this region, precipitation over south Brazil and Uruguay – hereafter called southeastern South America (SESA) – is quite uniform throughout the year, contrary to most of the continent which has a marked seasonal cycle in rainfall amounts. Nevertheless, the mechanisms for rainfall production in SESA are seasonally dependent: frontal systems dominate during the cold season, while deep convection dominates during the warm season even though there are still fronts reaching the region and are important for precipitation production (Garreaud and Aceituno, 2007; Catto *et al.*, 2012).

While SESA is often treated as a uniform region to study its predictability due, e.g. to El Niño–Southern Oscillation (ENSO; e.g. Ropelewski and Halpert, 1987; Barreiro and Tippmann, 2008; Barreiro, 2010), some studies have shown that the northern part behaves differently from the southern region, the limit being close to the latitude of the Negro river in the middle of Uruguay (about 33°S, see Figure 1). In particular, the northern region (north of Uruguay and south Brazil) has a strong and consistent ENSO impact, while the southern region has a much weaker ENSO impact (e.g. Pisciottano *et al.*, 1994; Grimm *et al.*, 2000). This results in higher seasonal predictability in northern Uruguay than in the south, in particular during spring and summer, allowing forecasts to be potentially useful for applications in the northern region (Berri *et al.*, 2005). The reasons for this different behaviour, though hypothesized due to the different role for frontal systems in organizing and producing rainfall, have not been explicitly addressed. This study aims at closing this gap through studying the interannual variability of atmospheric transients that affect SESA rainfall during summer.

Given their importance in the development of surface weather such as cyclogenesis, there is a large literature about the trajectories of atmospheric transients. Some

*Correspondence to: M. Barreiro, Departamento de Ciencias de la Atmósfera, Facultad de Ciencias, Universidad de la Republica, Iguá 4225, Montevideo 11400, Uruguay. E-mail: barreiro@fisica.edu.uy

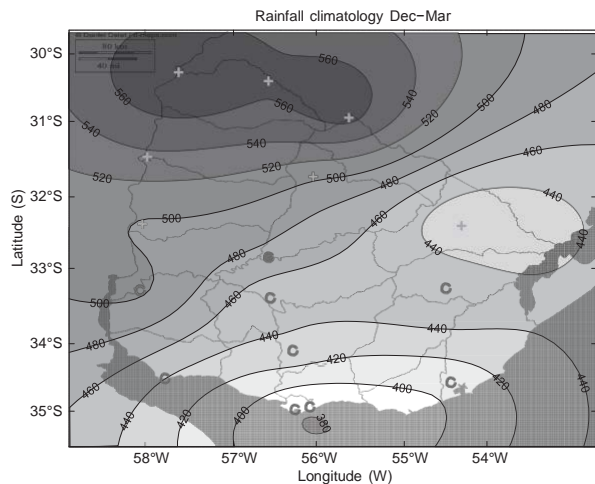


Figure 1. Climatological accumulated rainfall during DJFM in Uruguay (mm). Also shown are the meteorological stations used in this study. Stations in the northern region are marked with crosses; stations in the southern region are marked with open circles. The limit between northern and southern Uruguay is at about 33°S. The station marked with a filled circle is neither considered to be in the northern nor in the southern region.

studies for the Southern Hemisphere (SH) include Trenberth (1981, 1982, 1991), Berbery and Vera (1996), Rao *et al.* (2002) and Nakamura and Shimpo (2004).

Chang and Yu (1999) developed an efficient methodology to track preferred paths of transient eddy and wave-packet propagation, group speed and wave coherence. Focusing on climatological aspects, they found that during summertime the SH shows only one waveguide that circles the globe between latitudes 50°–60°S. Moreover, on average transients propagate along this waveguide with a group velocity of about 20–25 m s⁻¹ so that a wave packet propagates around the latitude circle in 2 weeks (Chang, 1999). Chang (2000) also showed that upper-level troughs associated with the wave packets were almost always associated with a surface cyclone developing just to the east. On interannual time scales, Solman and Menendez (2002) characterized the variability of winter storm tracks using the meridional winds at 300 hPa over the south Pacific–south Atlantic sector. They found that during El Niño wave trains in the subtropical Pacific propagate along a northern path compared to La Niña events, consistent with an equatorward shift of the axis of maximum baroclinicity.

ENSO also affects SESA rainfall during summer, and many studies have shown that the mechanisms involve both upper and lower level atmospheric circulation anomalies. The Appendix provides a summary of the anomalies associated with ENSO. During El Niño, the northerly flow from the Amazon basin strengthens increasing the availability of moisture south of 20°S (e.g. Silvestri, 2004). In upper levels, the strengthening and meandering of the subtropical jet due to stationary Rossby wave trains forced from the equatorial Pacific increases baroclinicity and the advection of cyclonic vorticity over SESA (Yulaeva and Wallace, 1994; Grimm *et al.*, 2000). These circulation

anomalies provide in turn the dynamic lift for convection initiation in an unstable environment maintained by the northerly advection of heat and moisture favouring the occurrence of mesoscale convective complexes (MCCs) in the region (e.g. Velasco and Fritsch, 1987; Satyamurty *et al.*, 1998; Salio *et al.*, 2007). However, this explanation does not explicitly mention changes in synoptic transients and their possible role in rainfall anomalies. Thus, this study has a twofold objective:

- Describe the interannual variability of transient energy propagation in extratropical South America during southern summer, relating it to changes in rainfall.
- Determine changes in transient energy propagation during ENSO with a focus on the different impacts over northern and southern Uruguay.

We will show that rainfall over the southern region of Uruguay is influenced by northward–southward shifts in the transient wave energy related to changes in the position of the subtropical jet. In addition, we found that in order for El Niño to induce rainfall anomalies in southern Uruguay and the Buenos Aires province transient activity must be increased between 35° and 45°S and moisture flow anomalies should reach southern Uruguay. Only some El Niño events produce a strong anticyclone off south Brazil that generates stronger northerly winds that bring moisture up to southern Uruguay. These El Niños also shift the subtropical jet southward, increasing transient activity in 35°–45°S. We hypothesize that the fronts associated with moving disturbances tap the increased moisture supply from the north creating positive rainfall anomalies in southern Uruguay.

The study is structured as follows. In the following section, we describe the data used and the methodology employed to characterize transient wave activity – the group velocity. In Section 3 the interannual variability of the extratropical group velocity is characterized in terms of empirical orthogonal functions (EOFs), which are then related to rainfall over Uruguay in Section 4. In Section 5 we calculate the covariability patterns between subtropical rainfall and the extratropical group velocity, and compare them to the average ENSO signal. Section 6 summarizes the main findings.

2. Data and methodology

2.1. Data

We use both daily and monthly mean data from the NCEP_Reanalysis 2 data provided by the NOAA/OAR/ESRL PSD, Boulder, CO, USA, from their website at <http://www.esrl.noaa.gov/psd/> (Kanamitsu *et al.*, 2002). The horizontal resolution of the data set is 2.5° × 2.5° and the period considered spans from January 1979 to December 2014. We consider only the summer season defined as the period from 1 December to 31 March (DJFM season). The first year considered is the period December 1979–March 1980, and it is noted

in this study as year 1980; the last season considered is December 2013–March 2014, thus covering a total of 35 years.

Daily mean meridional velocity at 300 hPa is used to represent upper level transient behaviour and to calculate the transient group velocity, as several previous studies have considered (e.g. Chang, 2000; Solman and Menendez, 2002). As wave energy propagates with the group velocity, we can consider this quantity as a measure of transient wave activity. The methodology to calculate the seasonal average group velocity for individual years is explained in Section 2.2. Once calculated, the interannual variability of the group velocity is analysed using EOFs and a maximum covariance analysis (MCA) with the precipitation. While the EOFs and their corresponding principal components (PCs) provide a way to characterize the main patterns of interannual variability of the group velocity, the MCA provides patterns of covariability between the group velocity and rainfall together with an index of time evolution for each pattern. As the MCA is based on the singular value decomposition (SVD), we will refer to the covariability modes as SVDs.

In order to understand the circulation anomalies associated with interannual changes in the transient wave energy we regressed seasonal mean anomalies of geopotential height at 300 hPa, winds at 300 and 850 hPa, sea surface temperature (SST) and precipitation onto the time series associated to the SVDs. SST data is taken from the Extended Reconstructed SST (ERSST) version 4 (ERSSTv4) data set (Huang *et al.*, 2015). The Nino3.4 index [SST average within (170–120°W, 5°S–5°N)], calculated using ERSSTv4 data, is constructed to characterize the ENSO phenomenon.

We consider two data sets for monthly mean rainfall. We use precipitation from the Global Precipitation Climatology Project (GPCP v2.2) from 1979 to 2014, which combines observations and satellite rainfall data into $2.5^\circ \times 2.5^\circ$ global grids (Adler *et al.*, 2003). This data set was also taken from the website of NOAA/OAR/ESRL PSD, Boulder, CO, USA. Owing to its global coverage, this data provides a complete view of precipitation anomalies associated with changes in transient wave energy. On the other hand, the low resolution prevents from looking into regional details. Thus, to better look at rainfall anomalies over Uruguay, we use monthly mean station data from the National Weather Service of Uruguay (INUMET) also during the period 1979–2014. The data set comprises 16 stations covering the whole country and their distribution is shown in Figure 1.

As mentioned in the Section 1 the northern and southern parts of Uruguay present different interannual variability and understanding their differences represents one of the main objectives of this work. Figure 2 clearly shows that the ENSO influence is concentrated in the northern sector of Uruguay, to the north of 33°S . Thus, with this result in mind this study considers the northern (southern) region of Uruguay as that located to the north (south) of 33°S . The stations located in northern (southern) Uruguay are shown as crosses (circles) in Figure 1. The station located at about

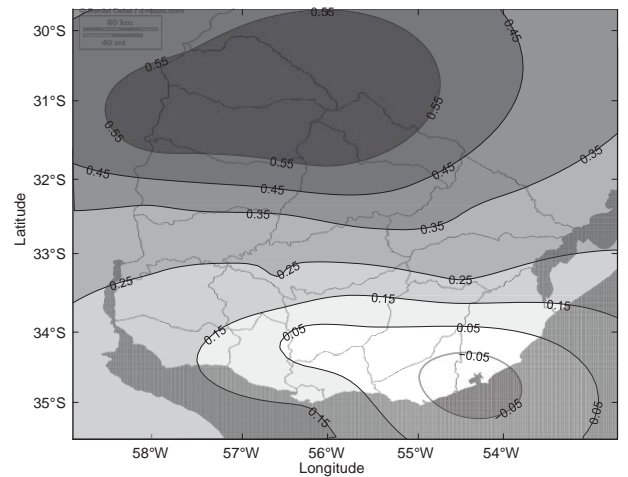


Figure 2. Correlation map between rainfall at stations of Figure 1 and Nino3.4 index during DJFM season. Values larger than 0.35 are significant at 5% level.

(56.5°W , 32.9°S) is neither considered to be in the northern nor in the southern region. Figure 1 also shows that the northern region receives on average accumulated rainfall amounts of 450–550 mm during DJFM season, while the southern region receives between 400 and 450 mm. The interannual correlation between rainfall from station data averaged in southern Uruguay with those averaged in northern Uruguay is 0.63, and thus the regions have only about 40% of the variance in common.

The statistical significance of the regression maps is assessed using a two-sided *t*-test. Correlation values are considered significant if they pass the test at 5% level.

2.2. Methodology to characterize atmospheric transients

The transient activity is characterized by the group velocity calculated following Chang and Yu (1999). To do so we use daily mean data of meridional velocity at 300 hPa, and since we are interested in transient waves we removed the stationary component by removing the DJFM mean from each summer season. As in Chang and Yu (1999) and Berbery and Vera (1996) we do not further filter the data.

To compute the group velocity we proceed as follows:

1. We compute envelopes of Rossby wave packets using the Hilbert transform method of Zimin *et al.* (2003) keeping wave numbers 4–11 as it has been shown these are representative of the transient waves in the SH (Trenberth, 1981). This results in a field of amplitudes for each day of the season.
2. We estimated the group velocity by performing one point time-lagged correlation maps of the amplitude of the envelope for each point in the domain (160°W – 40°E , 70°S – 10°N). The zonal and meridional components of the group velocity at each location were estimated from the displacement in the position of the correlation maximum from time lag of day -1 to day $+1$. As a sensitivity test, we used the maximum correlation values at days -2 and $+2$, and results turned out to be very similar. As result, we obtained

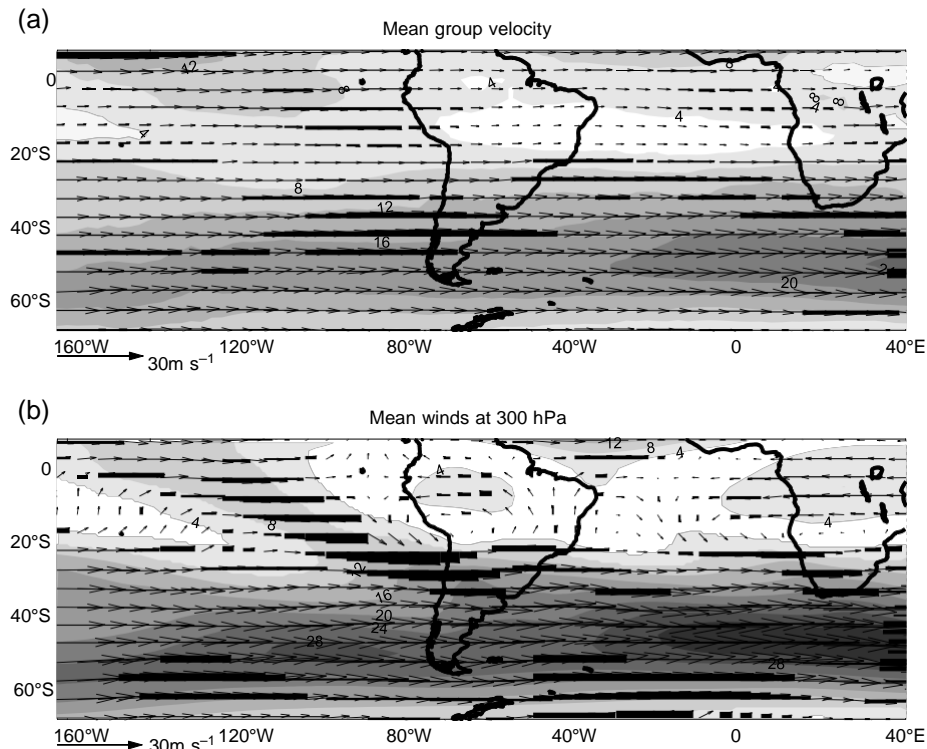


Figure 3. (a) Mean group velocity during DJFM season and (b) climatology of 300 hPa winds for DJFM season. The shading interval is 4 m s^{-1} .

a field of transient group velocity for each year in the region, which represents the average behaviour in the propagation of wave energy during each DJFM season. This field is used to study interannual variability.

The mean group velocity averaged over all 35 years is shown in Figure 3(a). Values are similar to those found in previous studies, with maxima of about 20 m s^{-1} between 50° and 60°S (Chang, 2000) in the extratropical wave guide (Figure 3(b)). In the Tropics the group velocity is relatively small, except for the eastern Pacific where it shows values of about 10 m s^{-1} and have a southward component, reflecting the propagation of waves from the Northern Hemisphere into the SH through the westerly duct.

3. Interannual variability of transient activity in the southeast Pacific–southwest Atlantic sector

To characterize the variability of the transient activity, we computed the EOFs of the zonal group velocity, given that it is the predominant direction. We focus on the region defined by 25° – 50°S and 130° – 30°W in order to better capture the dynamics of transients that influence subtropical precipitation. The variability of the zonal group velocity is maximum in the subtropical Pacific in a northwest–southeast direction, and in southwestern Atlantic Ocean at about 40°S (Figure 4(a)).

The first three EOFs explain 22, 14 and 12% of the total variability, respectively (the fourth EOF is well separated and only explains 7%), thus describing together about half of the total variance. The spatial patterns and associated

PCs of the EOFs are shown in Figure 5. Note that the PCs show strong interannual variability and no linear trend.

The leading EOF depicts a change in the amplitude of transient activity in the subtropical Pacific west of 100°W that extends with smaller amplitude into the South American continent to the north of 30°S . The associated PC1 shows interannual variability with only one strong negative value during year 1998. The pattern of EOF2 represents mainly a strengthening (weakening) of transient activity to the north (south) of 35°S in the Pacific sector with weak anomalies over the South American continent. Finally, EOF3 shows a southward shift of transient activity that extends from the Pacific into South America and the Atlantic Ocean south of 35°S . The line dividing the decrease–increase in transient activity is at about 33°S over the continent, just at the latitude of Uruguay. The PC3 shows 6 years of large positive anomalies while in most of the rest of the years it presents small negative values.

To determine the possible relationship between the EOFs and the principal modes of climate variability in the SH, we correlated the corresponding PCs with Nino3.4 and to an index of the Southern Annular Mode (SAM, taken from NOAA website http://www.cpc.ncep.noaa.gov/products/precip/CWlink/daily_ao_index/aao/aao_index.html). We found that none of the PCs are significantly correlated with the SAM, which may be due to the fact that SAM presents large monthly variability within the season. On the other hand, the leading two EOFs are significantly correlated to ENSO (Table 1). They suggest that during the warm (cold) phase of ENSO there is an increase and northward shift (decrease and southward

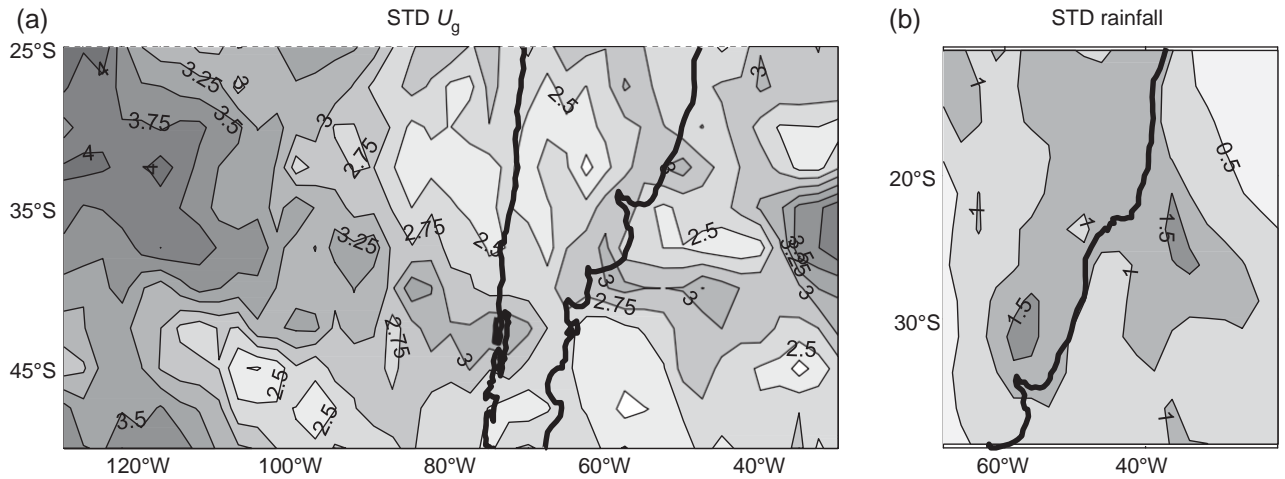


Figure 4. Interannual standard deviation during DJFM for the (a) zonal group velocity (m s^{-1}) and (b) GPCP rainfall (mm day^{-1}).

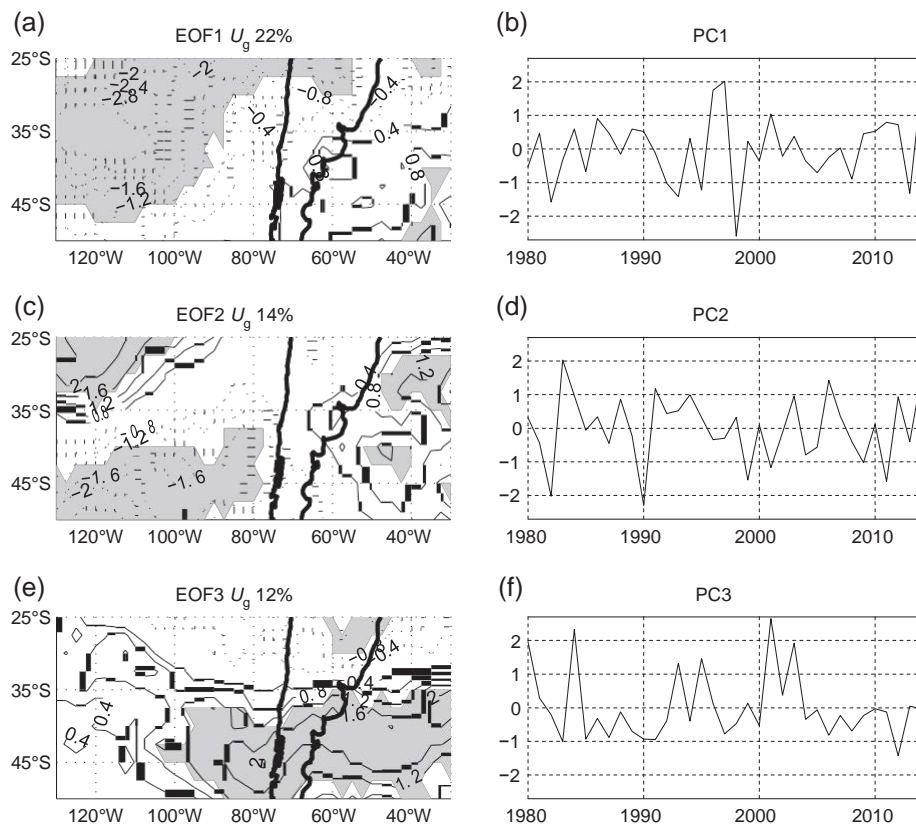


Figure 5. EOFs of the zonal group velocity: (a) and (b) show the leading EOF and the corresponding PC, (c) and (d) show the second EOF and PC, (e) and (f) show the third EOF and PC. Spatial patterns are in m s^{-1} , while the time series are normalized. Shading marks significance at 5% level.

shift) of wave activity in the subtropical Pacific that tends to extend into South America north of 30° S.

4. Relationship between rainfall over Uruguay and transient activity

As it was mentioned in Section 1, rainfall over Uruguay is strongly related to ENSO through the establishment of tropically forced stationary waves that will alter the regional atmospheric dynamics. While these anomalies

strongly affect northern Uruguay (mainly through an increase in MCC activity), rainfall in southern Uruguay shows no consistent relationship to ENSO (see Figure 2). In this section, we further investigate the different relationship between rainfall anomalies and transient activity for the northern and southern regions of Uruguay.

A correlation analysis between the PCs of U_g and the northern and southern regions of Uruguay shows that only the latter is significantly correlated to transient activity, having a correlation value of 0.41 with PC3 (Table 1). This

Table 1. Correlation between PCs associated with the three leading EOFs of U_g and different indices used in this study. Northern (southern) Uruguay is an index constructed by averaging rainfall from station data located to the north (south) of 33°S (see text).

Statistically significant values are shown in bold.

	PC1	PC2	PC3
Niño3.4	-0.40	0.34	0.04
SAM	0.06	-0.28	-0.27
Northern Uruguay	-0.21	0.17	0.18
Southern Uruguay	0.05	0.05	0.41

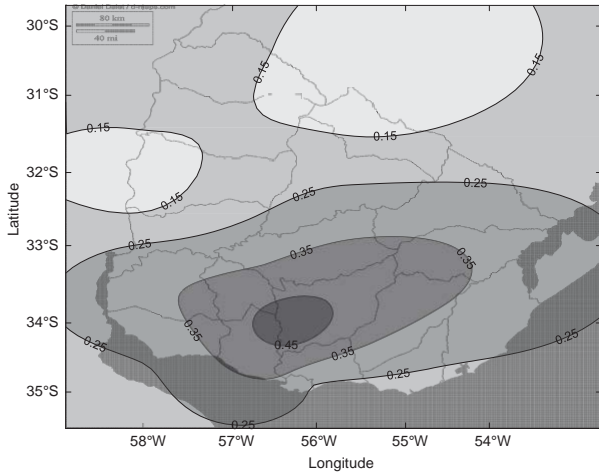


Figure 6. Correlation of PC of EOF3 of U_g with rainfall in meteorological stations in Uruguay. Values larger than 0.35 are significant at 5% level.

is further shown in Figure 6, where we plot the correlation between the PC3 of U_g and rainfall at each station over Uruguay. Clearly, rainfall anomalies are significantly correlated with changes in transient activity only to the south of 33°S , while to the north there is a correlation close to zero. Comparison with Figure 2 stresses the different behaviour of interannual rainfall variability in northern and southern Uruguay.

To add support to above findings Figure 7 shows the correlation maps during DJFM between the zonal group velocity (U_g) and rainfall from station data averaged in the southern and northern regions of Uruguay, as well as with the Niño3.4 index. As in the previous analysis, correlations are mainly significant with the zonal group velocity and those with the meridional velocity are not shown. In the case of southern Uruguay the increase in precipitation is accompanied by an increase in U_g between 35° and 40°S that extends from the south Pacific towards the Atlantic, consistent with the EOF3 of U_g (Figure 7(a)). Moreover, the pattern suggests a southward shift of transient activity over all the south Atlantic basin.

In the case of the northern Uruguay region the correlation is significant in the eastern Pacific at about 20°S and between 35° and 40°S , but the pattern does not extend over South America (Figure 7(b)). In fact, the spatial structure of the correlation is similar to that between U_g and Niño3.4 (Figure 7(c)), a somewhat expected result given

that rainfall in the northern region of Uruguay is strongly correlated with ENSO. Note that northern Uruguay is not significantly correlated to the EOF1 of U_g (nor with EOF2, nor EOF3, Table 1), which is not inconsistent given that most of the weight of EOF1 is in the central Pacific. The similarity between Figures 7(a) and (b) is not large and, in particular, there is total absence of the maximum correlation in the tropical eastern Pacific at about 20°S in Figure 7(a), which stresses the dependence of southern Uruguay on subtropical transient dynamics.

To test whether the group velocity is characterizing adequately changes in storm tracks we compared the results using this diagnostic with another one more commonly used, namely, the eddy kinetic energy (K). Analogous correlation maps of K with Uruguayan rainfall and Niño3.4 show that the results are not sensitive to the used diagnostics (Figure 8): southern Uruguay rainfall is strongly correlated with a southward shift in the storm track, while northern Uruguay is correlated to ENSO.

These results reinforce the idea that northern Uruguay is only weakly associated to transient frontal activity, but instead is mainly related to the development of MCCs which frequency of occurrence is modulated by the large scale conditions. As mentioned in the literature, during El Niño the increase in low level moisture from the north and upper level advection of cyclonic vorticity and a stronger jet (see Appendix) increase the vertical shear providing dynamical favourable conditions to the development of MCCs. Davison (1999) also pointed out that a stronger jet crossing the Andes leads to increased shortwave perturbations which help initiate MCCs.

5. Covariability between transient activity and rainfall in SESA

A MCA between the seasonal mean (DJFM) rainfall and the group velocity (V_g) is performed to better characterize the coupled interannual variability. The analysis is performed for GPCP rainfall within the region (70° – 50°W , 40° – 25°S) and group velocity within (130° – 30°W , 50° – 25°S) (the same as for the EOF analysis). As Figure 4(b) shows, SESA is the continental region with maximum interannual rainfall variability. The spatial patterns computed considering only the zonal component of the group velocity are almost the same as using both components and explain almost the same amount of covariability. Thus, the variability of V_g is mainly that associated with U_g .

The leading MCA mode (SVD1) explains 56% of the covariance and shows increased rainfall in SESA with maximum anomalies over northern Uruguay and southern Brazil concurrent with a small decrease in rainfall in the South Atlantic Convergence Zone (SACZ) region (Figure 9). A similar positive correlation pattern is seen for rainfall station data in Uruguay (not shown). The accompanying group velocity anomalies show a clear strengthening of transient energy in a region that extends continuously from the southeast Pacific towards the south

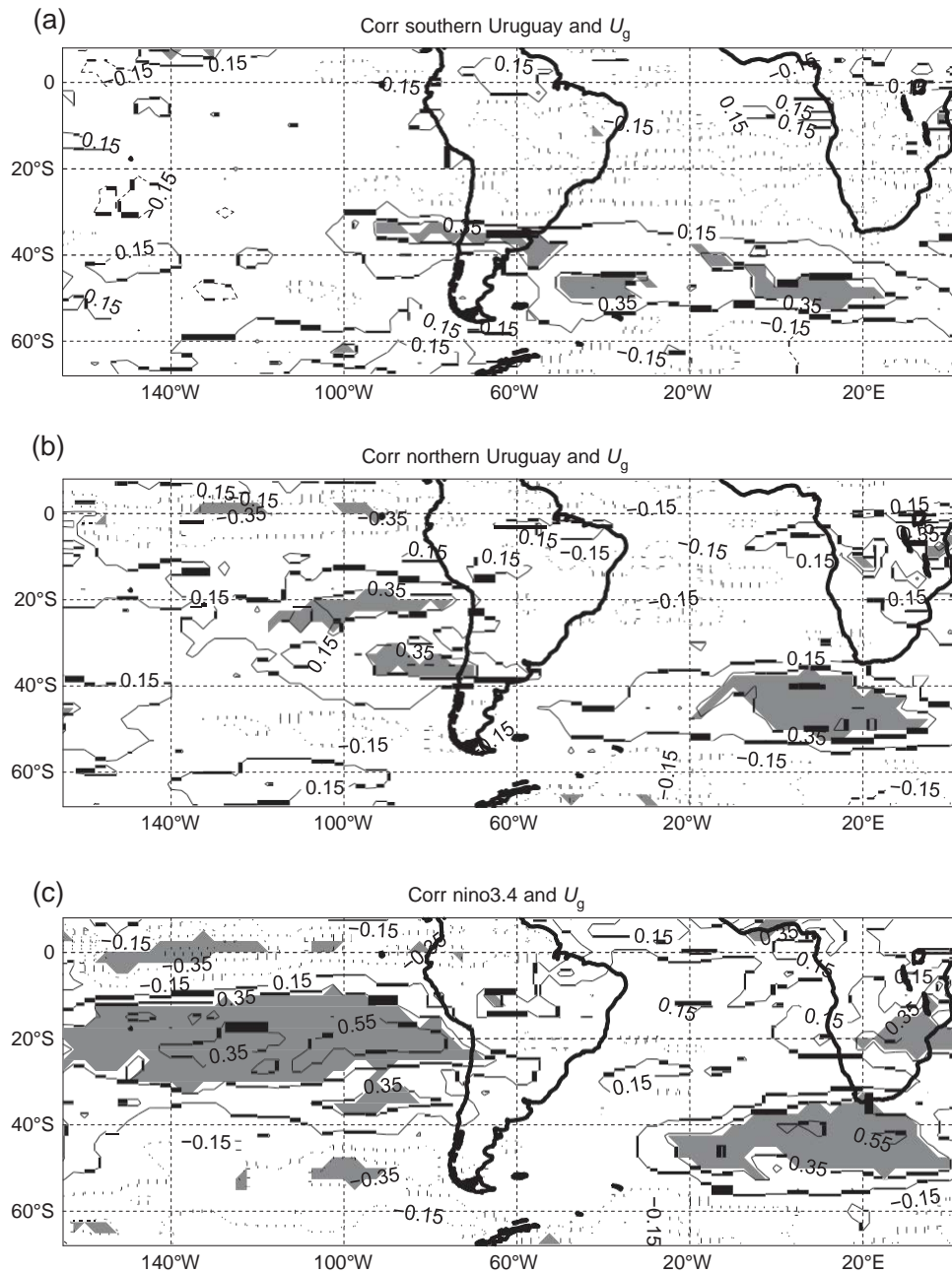


Figure 7. (a) Correlation between rainfall averaged over the stations located in the southern region of Uruguay and the zonal group velocity. (b) Idem but for rainfall averaged over the northern region of Uruguay. (c) Idem but for Nino3.4 index. Shading denotes significant correlations at 5% level.

Atlantic and small decreased transient energy in the SACZ region. The anomalies are mainly zonal and the spatial pattern looks very much like EOF3 of U_g (the corresponding PCs are correlated at 0.71). The time series show strong interannual variability clearly related to the central equatorial Pacific, where correlations are maximum. The time series of V_g is also correlated to the SAM index at $r = -0.34$, that is just significant at 5% level.

Regression of other fields onto the time series associated to V_g show the ENSO signature in the Tropics and the associated extratropical teleconnections. In particular, the low-level wind anomalies in the south Atlantic represent a weakening of the anticyclone which decreases the trades (leading to decreased oceanic heat loss) and is the most

likely cause for the warm oceanic anomalies north of 30°S (Figure 10(a)). In the extratropical Pacific low-level wind anomalies are also consistent with atmospheric forcing of SST anomalies seen in Figure 9(d).

Over continental South America, there is a clear increase in the seasonal mean winds from the Amazon basin towards SESA that supply enhanced moisture to the region. Note that this low-level wind anomalies are much stronger than in the ENSO regression shown in Figure A1 and extend further into southern Uruguay. Moreover, the increased continental northerlies connect to the cyclonic circulation in the south Atlantic, which centre is located at about 10°W , westward from the one seen in the ENSO regression map (Figure 10(a)).

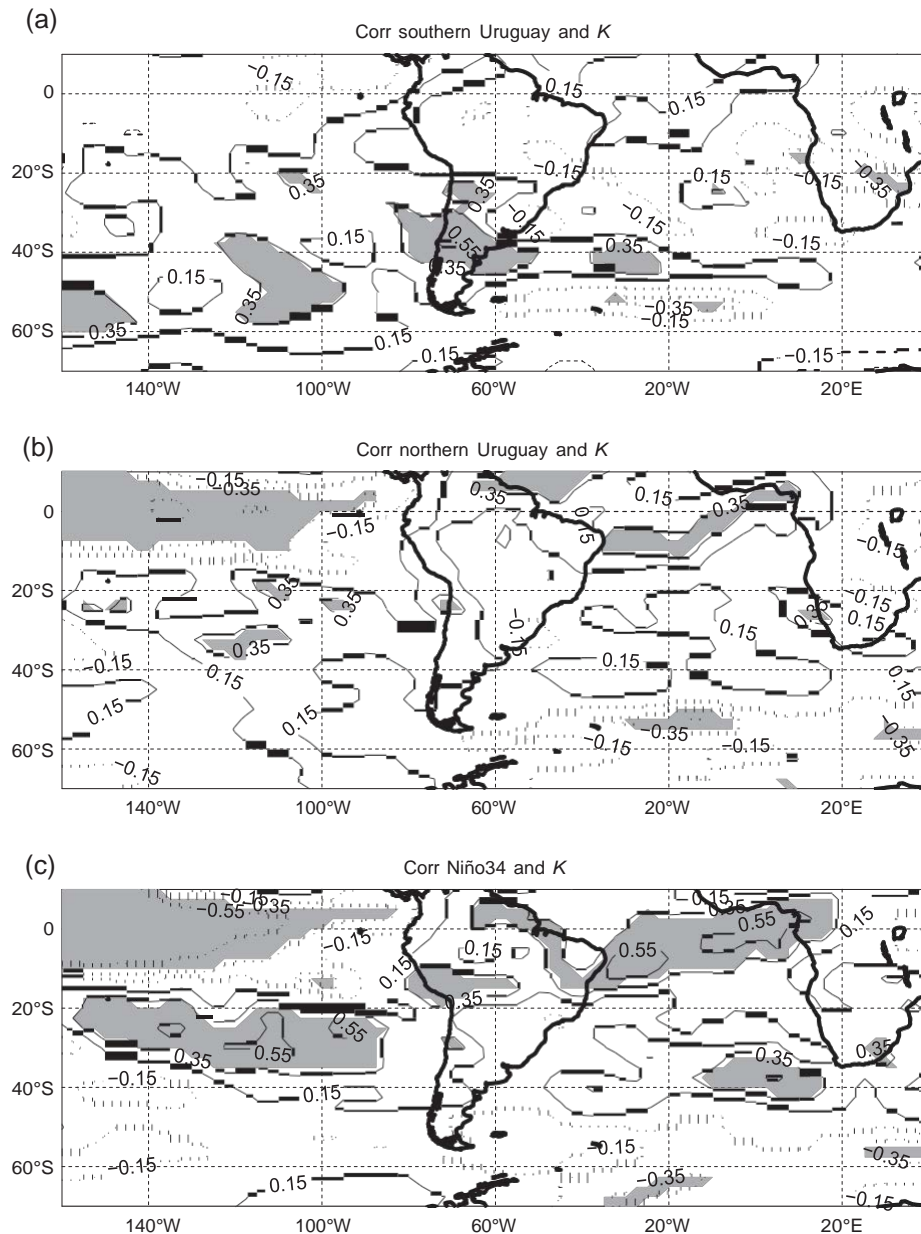


Figure 8. Idem to Figure 7 but for the eddy kinetic energy, K .

In upper levels anomalies over SESA are dominated by an anticyclonic circulation centered off south Brazil and increased westerlies south of 35°S that extend over the whole south Atlantic basin suggesting a southward shift of the subtropical jet (Figure 11(a)). In fact, this increase in the winds over the Atlantic seems to be connected with the subtropical increase in the Pacific basin, thus generating a wave guide through which the enhanced transient activity propagates as seen in the anomalies of V_g (Figure 9(b)). North of 35°S the wind anomalies tend to meander showing a trough west of the Andes which, together with the anticyclone east of the Andes, increases the advection of cyclonic vorticity by the subtropical jet and provides dynamical favourable conditions for ascent. Thus, similar to the average influence of ENSO, the seasonal mean anomalies show upper level and lower level

conditions favourable for rainfall in south Brazil and north of Uruguay, thus explaining the observed strong rainfall anomaly there.

On the other hand, the increased transient activity south of 35°S seen in SVD1, but not in the average ENSO regression, together with the southward extension of the anomalous northerly winds, are the main responsible for the increased rainfall in southern Uruguay and the Buenos Aires province of Argentina. We hypothesize that increased frontal activity associated with the travelling disturbances organizes convection in an environment that has become more unstable due to the enhanced moisture and warm air brought by the strengthened northerlies (Seluchi and Chou, 1999). Thus, fronts induce positive rainfall anomalies in southern Uruguay. In addition, these fronts will be blocked by the anomalous anticyclone off Brazil, so

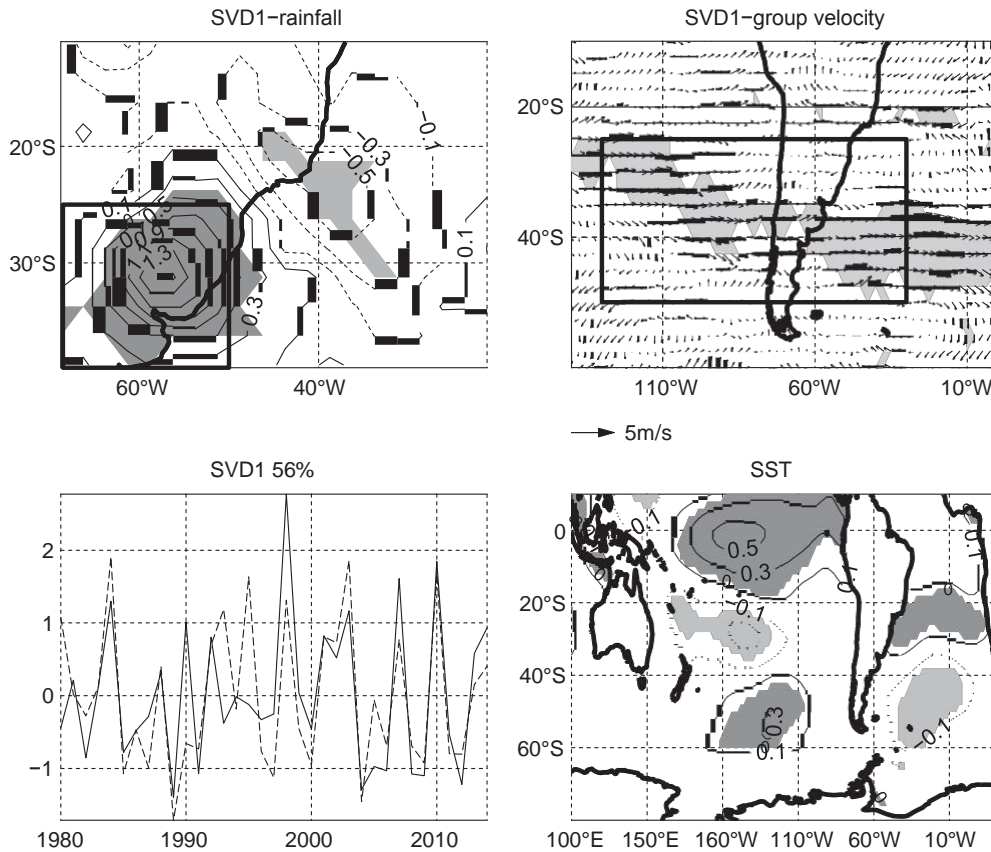


Figure 9. Leading SVD (SVD1) between rainfall and V_g . (a) Rainfall mm day^{-1} , (b) group velocity, (c) associated normalized time series for rainfall (solid) and for group velocity (dashed) and (d) regression of SST anomalies onto the time series of V_g . In panels shading denotes regions statistically significant. In (a) and (b) boxes mark the regions used to perform the MCA.

that they cannot propagate northward thus explaining the decrease in transient activity in the SACZ region (Satyamurty *et al.*, 1998).

It is worth noting that Ungerovich and Barreiro (2015) constructed a dynamical-statistical model for summertime rainfall prediction over southern Uruguay that showed considerable skill. They used as predictors meridional winds at 200 hPa in the region ($60^\circ\text{--}40^\circ\text{W}$, $10^\circ\text{--}33^\circ\text{S}$) and zonal winds at upper and lower levels in the band $25^\circ\text{--}40^\circ\text{S}$. These predictors characterize the strong anticyclone off south Brazil and the increased zonal flow that are seen in the regression maps of SVD1 (Figures 10(a) and 11(a)), and thus are consistent with the results presented here.

The second MCA mode (SVD2) explains 16% of the covariance and mainly shows a dipole of rainfall with positive anomalies over south Brazil and negative in eastern Argentina and to the south of Uruguay, presenting the largest anomaly gradient over Uruguay (Figure 12). A similar north–south rainfall anomaly pattern is seen for station data in Uruguay (not shown). Regression onto SST anomalies shows positive correlation in the eastern Pacific and the extratropical oceans. The group velocity shows strengthened transient energy in the southeast Pacific extending towards subtropical South America at about 30°S and into the Atlantic basin. The spatial pattern of V_g is dominated by zonal group velocity anomalies, and it looks very

similar to EOF1 of U_g (with changed sign, Figure 5) being the PCs correlated at -0.9 .

Upper level winds show a strengthened subtropical jet at about 30°S extending from the Pacific into the continent and, differently from the SVD1 case, shows no meandering (Figure 11(b)). These circulation anomalies suggest an equatorward shift of the subtropical jet and the storm track over South America during some El Niño years. However, contrary to the average ENSO regression, low level winds show no significant changes over South America (see Figures 10(b) and A1(b)).

Comparing the circulation anomalies associated with the first and second SVDs, it is clear that different stationary waves forced from the tropical Pacific induce different configurations at upper and lower levels. This is best seen in the 300 hPa geopotential height anomalies (Figure 11). While in SVD1 there are clearly two waves emanating from the tropical Pacific towards the SH extratropics – one emanates from the central Pacific describing a long arch and another shorter one emanates from the eastern Pacific creating the anticyclone off south Brazil – in the SVD2 there is only one forced wave. Comparing the spatial structures, it is evident that the regression of SVD2 lacks the short wave that emanates from the eastern Pacific and bends towards South America at the latitude of the subtropical jet. The absence of this stationary wave allows the wave emanating from the central Pacific to be displaced

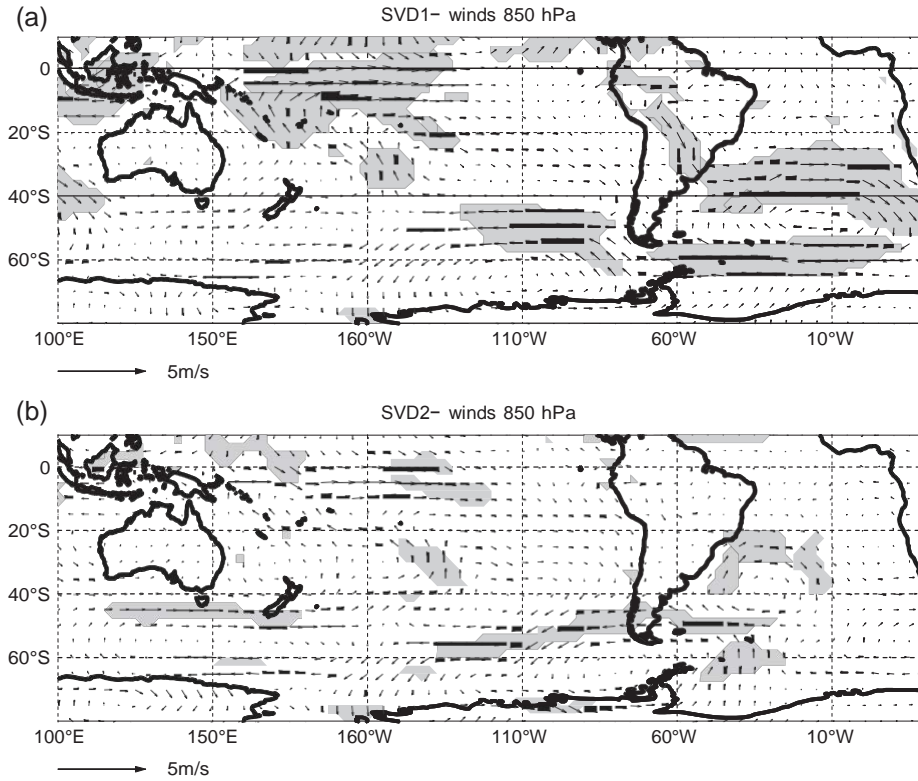


Figure 10. Regression of 850 hPa winds onto the time series associated to V_g of (a) SVD1 and (b) SVD2. Shaded areas are significant at the 5% level.

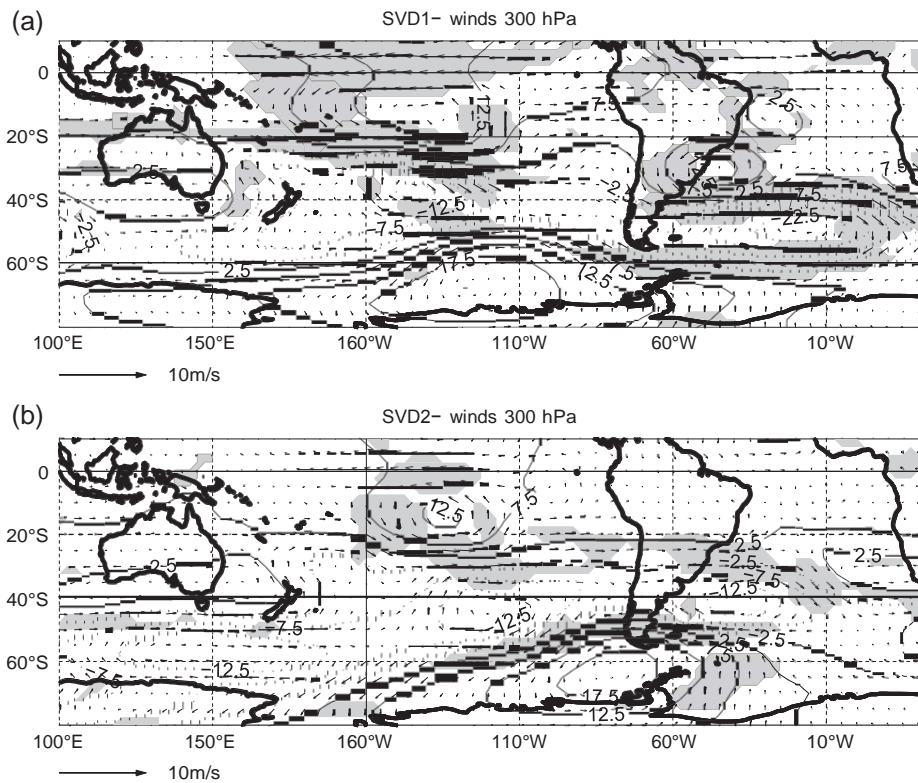


Figure 11. Regression of winds and geopotential height (m) at 300 hPa onto the time series associated to V_g of (a) SVD1 and (b) SVD2. Shaded areas indicate significance of wind anomalies at the 5% level.

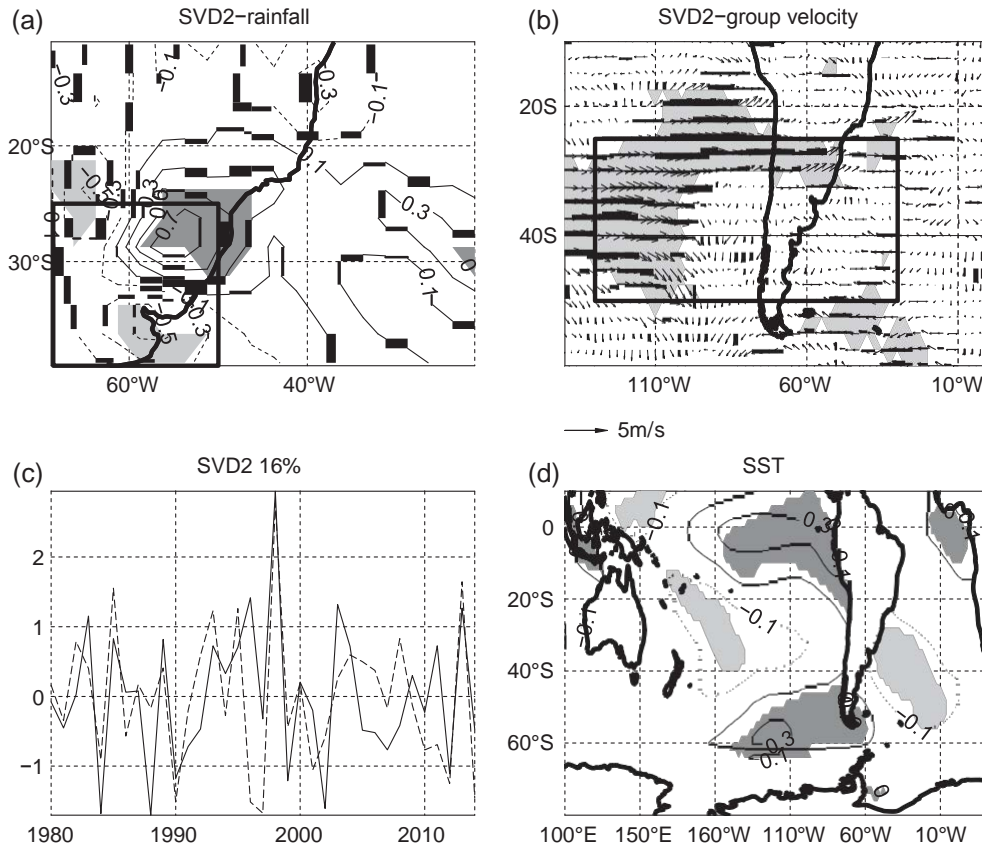


Figure 12. Idem to Figure 9 but for the second SVD (SVD2) of rainfall and group velocity.

eastward with respect to the pattern in SVD1. This generates very different regional anomalies in SESA. While in SVD1 regional anomalies are dominated by the anticyclone off Brazil, in SVD2 there is not such feature and instead, wind anomalies are dominated by a cyclonic anomaly off the coast of Argentina. As result, in SVD2 upper level wind anomalies strengthen at 30°S consequence of the two cyclonic anomalies centered in the eastern Pacific and western Atlantic at 45°S . This strengthening represents a northward shift of the subtropical jet favouring transient energy propagation at 30°S which induces positive rainfall anomalies at these latitudes, as well as decreased rainfall to the south. The increase in transient activity reaches into the Atlantic favouring enhanced rainfall in the oceanic extension of the SACZ.

These results suggest that the pattern of SST anomalies during El Niño years is important for inducing summertime rainfall anomalies over Uruguay. As an example, we compare two El Niño events: 2010 – characterized by SST anomalies in the central Pacific – and 1983 – characterized by maximum anomalies in the eastern Pacific. Figure 13 shows the rainfall anomalies for El Niño of 2010 when a positive rainfall anomaly covered all Uruguay, and for El Niño of 1983 when excess rainfall was weaker and limited to south Brazil and northern Uruguay; southern Uruguay, instead, showed a negative rainfall anomaly. Regarding SVD1, El Niño of 1983 has zero amplitude in the PCs of rainfall and V_g , while El Niño of 2010 has large positive values in both of them. On

the contrary, in SVD2 year 1983 presents positive values of PCs, while 2010 shows negative amplitudes. Thus, these amplitudes are in agreement with the patterns of SST and rainfall anomalies that characterize each El Niño event, and demonstrate that the first two SVDs capture the main rainfall variability in SESA and its relationship with circulation anomalies. Note that El Niño of 1998 shows large positive values in both SVDs, thus suggesting that the observed strong rainfall anomalies over south Brazil and northern Uruguay were due to large changes in the regional circulation that include anomalous stationary waves and enhanced transient activity.

6. Summary

In this study, we explored the interannual variability of transient activity during SH summer in the extratropical sector of the south Pacific and Atlantic oceans. Having in mind that subtropical South America is a transition region between a convection-dominated regime and one where frontal activity dominates we assessed the degree to which transient activity accounts for rainfall anomalies over SESA focusing on Uruguay. In spite of the relatively small area, on interannual time scales rainfall in the northern and southern regions are only correlated at 0.63 during southern summer, thus suggesting that different physical processes govern these two regions. This is exemplified by the fact that, different from the north, southern Uruguay

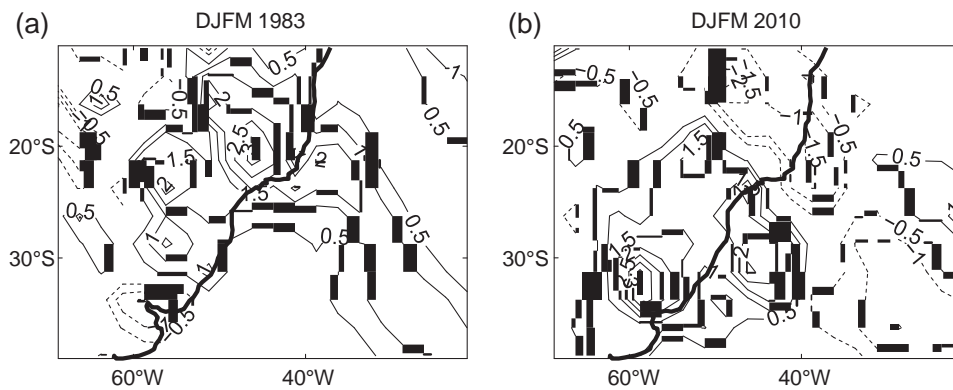


Figure 13. Rainfall anomalies in mm day^{-1} during El Niño events of (a) 1983 and (b) 2010.

does not show a consistent response to ENSO events. To accomplish these tasks we calculated the group velocity of wave packets as a measure of transient activity, following the methodology developed by Chang and Yu (1999) together with the procedure of Zimin *et al.* (2003) to compute wave envelopes.

We found that extratropical transient activity shows strong interannual variability consisting in patterns that represent (1) a change in the intensity of wave activity in the subtropical Pacific and (2) meridional shifts in the position of the Pacific and Atlantic storm tracks. The leading two modes of variability are associated with ENSO. The third mode of variability represents latitudinal shifts in transient wave activity such that a southward movement of the storm track enhances rainfall over southern Uruguay. The southward shift consists of a strengthening in transient energy south of 35°S extending from the southeastern Pacific into the South American continent and south Atlantic.

To better understand the connection between rainfall anomalies over SESA and transient wave energy, we performed an MCA between these two fields. The leading SVD mode explains more than half of the covariability and represents the influence of the central equatorial Pacific on rainfall anomalies over SESA. It shows that for an El Niño event to induce positive rainfall anomalies over southern Uruguay (in addition to south Brazil and northern Uruguay) it has to force two stationary waves: a wave that emanates from the central Pacific and describes an arch with low curvature into higher latitudes and then towards the south Atlantic and another shorter wave that emanates from the eastern Pacific and turns north-eastward at the latitude of the subtropical jet (as in Grimm and Ambrizzi, 2009). When the induced anticyclone off Brazil is strong then surface northerlies will reach southern Uruguay destabilizing the atmosphere due to the enhanced transport of moisture and warm air. At the same time, changes in upper level winds strengthen the transient wave activity south of 35°S so that the increased associated frontal activity can induce positive rainfall anomalies by tapping the increased available moisture.

We also found that the equatorial Pacific could also force only one stationary wave from the central Pacific.

In opposition with the leading SVD mode where central Pacific SST anomalies played the larger role, in this latter situation eastern equatorial Pacific SST anomalies seem to be responsible. In this latter case, characterized by SVD2, the regional circulation over SESA is dominated by two cyclonic anomalies located in the eastern Pacific and western Atlantic centered at about 45°S . This configuration shifts the subtropical jet to the north of 30°S favouring increased rainfall over south Brazil and decreased rainfall to the south of Uruguay. Previous authors had found a dependence of the SH atmospheric circulation response to different types of El Niño events during spring (e.g. Vera *et al.*, 2004).

Overall, our results suggest that rainfall over southern Uruguay is dominated by transient activity even in SH summer, in contrast with northern Uruguay which is dominated by a deep convective regime during this season. This different dynamics stresses the fact that Uruguay is in a transition region and has strong consequences for rainfall predictability. While the northern region is strongly predictable during El Niño events mainly because it favours the development of MCCs, predictability in the southern region depends on changes in the trajectory of transients, which is controlled by the spatial pattern of SST anomalies in the equatorial Pacific.

As a final note we mentioned that in this study we have taken the view that changes in the transient activity can be understood in terms of an equatorial Pacific SST forcing of the mean flow through the propagation of stationary waves which in turn modify the paths of transient eddies. However, several studies have shown that the changes in transient eddies can in turn modify the mean flow in the extratropics through eddy momentum and heat flux anomalies (e.g. Held *et al.*, 1989). The identification of cause and effect in the adjustment of the mean and transient atmospheric circulation is beyond the scope of this study and is left for future work.

Acknowledgement

The author was partially supported by Agencia Nacional de Investigación e Innovación under grant no. FCE_1_2014_1_104539.

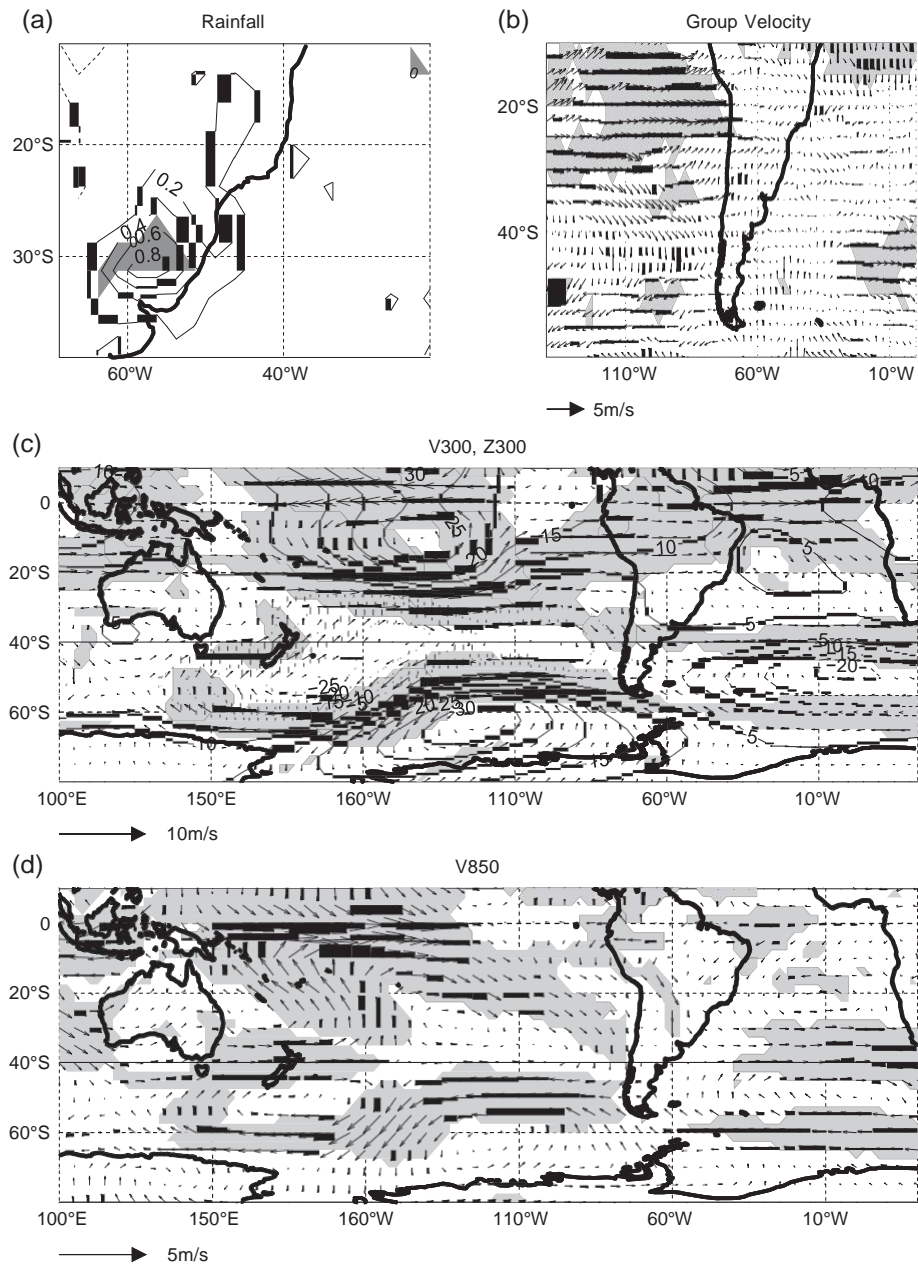


Figure A1. Regression of different fields onto Niño3.4 for DJFM season: (a) GPCP rainfall (mm day^{-1}), (b) group velocity, (c) winds and geopotential height (m) at 300 hPa and (d) winds at 850 hPa. Shading denotes significant correlations at 5% level. In (b) shading corresponds to wind anomalies.

Appendix: ENSO influence over SESA

In this section we review the average circulation anomalies over subtropical South America related to ENSO. To characterize ENSO influence we regressed different fields onto Niño3.4.

In agreement with Figure 2, there is a positive rainfall anomaly associated with El Niño statistically significant only over northern Uruguay and south of Brazil (Figure A1(a)). This has been shown to be a response to (1) increased northerly low-level winds that bring enhanced moisture from the Amazon and (2) increased advection of cyclonic vorticity in upper levels which provides the necessary dynamic lift (e.g. Grimm *et al.*, 2000; Silvestri, 2004). The latter anomalies are the result of the joint development

of a cyclonic anomaly in the southeast Pacific centered at about (40°S , 100°W) and an anticyclonic anomaly located off the coast of south Brazil and Uruguay (which, due to its barotropic structure, also induces northerly wind anomalies in the region). These in turn are part of a wave train that propagates from the eastern Pacific into the southern tip of South America which then turns north-eastward at the latitude of the subtropical jet towards the Atlantic (e.g. Grimm and Ambrizzi, 2009). The anomalies described are clearly seen in the low-level winds as well as in the 300 hPa winds and geopotential height fields (Figure A1). Apparent is also an additional wave emanating from the central tropical Pacific towards the extratropics with smaller curvature.

The regression also shows that there is enhanced transient activity in the tropical eastern Pacific up to 35°S (Figure A1(b)), in agreement with EOF1 of the zonal group velocity, but anomalies do not penetrate into the South American continent (see also Figure 7(c)). Consistently, this increased transient activity is accompanied by stronger upper level winds in the region. However, the regression map of 300 hPa winds also shows that the subtropical jet is intensified between 35° and 45°S over South America and the Atlantic Ocean, but the transient activity is not modified there.

References

- Adler RF, Huffman GJ, Chang A, Ferraro R, Xie P, Janowiak J, Rudolf B, Schneider U, Curtis S, Bolvin D, Gruber A, Susskind J, Arkin P. 2003. The version 2 Global Precipitation Climatology Project (GPCP) monthly precipitation analysis (1979-present). *J. Hydrometeorol.* **4**: 1147–1167.
- Barreiro M. 2010. Influence of ENSO and the South Atlantic Ocean on climate predictability over southeastern South America. *Clim. Dyn.* **35**(7–8): 1493–1508.
- Barreiro M, Tippmann A. 2008. Atlantic modulation of El Niño influence on summertime rainfall over southeastern South America. *Geophys. Res. Lett.* **35**(16): L16704, doi: 10.1029/2008GL035019.
- Berbery EH, Vera CS. 1996. Characteristics of the Southern Hemisphere winter storm track with filtered and unfiltered data. *J. Atmos. Sci.* **53**: 468–481.
- Berri GJ, Antico PL, Goddard L. 2005. Evaluation of the Climate Outlook Forums' seasonal precipitation forecasts of southeast South America during 1998–2002. *Int. J. Climatol.* **25**: 365–377.
- Catto JL, Jakob C, Berry G, Nicholls N. 2012. Relating global precipitation to atmospheric fronts. *Geophys. Res. Lett.* **39**: L10805, doi: 10.1029/2012gl051736.
- Chang EKM. 1999. Characteristics of wave packets in the upper troposphere. Part II: seasonal and hemispheric variations. *J. Atmos. Sci.* **56**: 1729–1747.
- Chang EKM. 2000. Wave packets and life cycles of baroclinic waves: examples from the Southern Hemisphere summer season of 84/85. *Mon. Weather Rev.* **128**: 25–50.
- Chang EKM, Yu DB. 1999. Characteristics of wave packets in the upper troposphere. Part I: Northern Hemisphere winter. *J. Atmos. Sci.* **56**: 1708–1728.
- Davison M. 1999. *Mesoscale Systems over South America*. Available from International Desks, National Centers for Environmental Prediction, Hydrometeorological Prediction Center/Development and Training Branch, 5200 Auth Rd., Camp Springs, MD 20746.
- Garreaud RD, Wallace JM. 1998. Summertime incursions of midlatitude air into subtropical and tropical South America. *Mon. Weather Rev.* **126**: 2713–2733.
- Garreaud RD, Aceituno P. 2007. Atmospheric circulation over South America: mean features and variability. In *The Physical Geography of South America*. Veblen T, Young K, Orme A (eds). Oxford University Press: Oxford, UK.
- Grimm AM, Barros VR, Doyle ME. 2000. Climate variability in southern South America associated with El Niño and La Niña events. *J. Clim.* **13**(1): 35–58.
- Grimm AM, Ambrizzi T. 2009. Teleconnections into South America from the Tropics and extratropics on interannual and intraseasonal timescales. In *Past Climate Variability in South America and Surrounding Regions: From the Last Glacial Maximum to the Holocene*, Vimeux F, Sylvestre F, Khodri M (eds). Springer: Apeldoorn, The Netherlands, 159–191, doi: 10.1007/978-90-481-2672-9_7.
- Held IM, Lyons SW, Nigam S. 1989. Transients and the extratropical response to El Niño. *J. Atmos. Sci.* **46**: 163–174.
- Huang B, Banzon VF, Freeman E, Lawrimore J, Liu W, Peterson TC, Smith TM, Thorne PW, Woodruff SD, Zhang H-M. 2015. Extended reconstructed sea surface temperature version 4 (ERSST.v4). Part I: upgrades and intercomparisons. *J. Clim.* **28**: 911–930.
- Kanamitsu M, Ebisuzaki W, Woollen J, Yang S-K, Hnilo JJ, Fiorino M, Potter GL. 2002. NCEP-DOE AMIP-II reanalysis (R-2). *Bull. Am. Meteorol. Soc.* **83**: 1631–1643, doi: 10.1175/BAMS-83-11-1631.
- Lenters JD, Cook KH. 1995. Simulation and diagnosis of the regional summertime precipitation climatology of South America. *J. Clim.* **8**: 2298–3005.
- Nakamura H, Shimpō A. 2004. Seasonal variations in the Southern Hemisphere storm tracks and jet streams in a reanalysis dataset. *J. Clim.* **17**: 1828–1844.
- Pisciottano GJ, Diaz AF, Cazes G, Mechoso CR. 1994. El Niño–Southern Oscillation impact on rainfall in Uruguay. *J. Clim.* **7**: 1286–1302.
- Rao VB, do Carmo AMC, Franchito SH. 2002. Seasonal variations in the Southern Hemisphere storm tracks and associated wave propagation. *J. Atmos. Sci.* **59**: 1029–1040.
- Ropelewski CF, Halpert MS. 1987. Global and regional scale precipitation patterns associated with the El Niño/Southern Oscillation. *Mon. Weather Rev.* **115**(8): 1606–1626.
- Salio P, Nicolini M, Zipser EJ. 2007. Mesoscale convective systems over southeastern South America and their relationship with the South American low-level jet. *Mon. Weather Rev.* **135**(4): 1290–1309.
- Satyamurty P, Nobre CA, Silva Dias PL. 1998. South America. In *Meteorology of the Southern Hemisphere*. American Meteorological Society: Boston, Massachusetts, USA, 119–139.
- Seluchi ME, Chou SC. 1999. Intercambio de masas de aire entre latitudes tropicales y extra tropicales de Sudamérica: Validación del modelo regional (in Spanish). *Climadlise* **14**(4): 1–26. <http://www.cptec.inpe.br/products/climanalise/artigos/articlen2.htm> (accessed 1 February 2016).
- Silvestri GE. 2004. El Niño signal variability in the precipitation over southeastern South America during austral summer. *Geophys. Res. Lett.* **31**: L18206, doi: 10.1029/2004GL020590.
- Solman S, Menendez C. 2002. ENSO-related variability of the Southern Hemisphere winter storm track over the eastern Pacific-Atlantic sector. *J. Atmos. Sci.* **59**: 2128–2140.
- Trenberth KE. 1981. Observed Southern Hemisphere eddy statistics at 500 mb: frequency and spatial dependence. *J. Atmos. Sci.* **38**: 2585–2605.
- Trenberth KE. 1982. Seasonality in Southern Hemisphere eddy statistics at 500 mb. *J. Atmos. Sci.* **39**: 2507–2520.
- Trenberth KE. 1991. Storm tracks in the Southern Hemisphere. *J. Atmos. Sci.* **48**: 2159–2178.
- Ungerovich M, Barreiro M. 2015. Seasonal forecast of accumulated rainfall in southern Uruguay during spring and summer. *Rev. Bras. Meteorol.* (in press).
- Velasco I, Fritsch JM. 1987. Mesoscale convective complexes in the Americas. *J. Geophys. Res.* **92**: 9591–9613, doi: 10.1029/JD092iD08p09591. ISSN: 0148-0227.
- Vera CS, Silvestri GE, Barros VR, Carril AF. 2004. Differences in El Niño response over the Southern Hemisphere. *J. Clim.* **17**: 1741–1753.
- Yulaeva E, Wallace JM. 1994. The signature of ENSO in global temperature and precipitation fields derived from the microwave sounding unit. *J. Clim.* **7**(11): 1719–1736.
- Zimin AV, Szunyogh I, Patil DJ, Hunt BR, Ott E. 2003. Extracting envelopes of Rossby wave packets. *Mon. Weather Rev.* **131**: 1011–1017.